catalysts

MDPI

Article

Cerium Doping Effect in 3DOM Perovskite-Type $La_{2-x}Ce_xCoNiO_6$ Catalysts for Boosting Soot Oxidation

Kaixuan Chen [1,†], Linsheng Xu [1,†], Yuanfeng Li [1], Jing Xiong [1], Dawei Han [1], Yaxiao Ma [1], Peng Zhang [1], Haoqi Guo [1] and Yuechang Wei [1,2,*]

[1] State Key Laboratory of Heavy Oil Processing, Key Laboratory of Optical Detection Technology for Oil and Gas, China University of Petroleum, Beijing 102249, China; 2022011859@student.cup.edu.cn (K.C.); xvlinsheng@163.com (L.X.); liyuanfeng@sust.edu.cn (Y.L.); xiongjing@cup.edu.cn (J.X.); 2021310806@student.cup.edu.cn (D.H.); mayaxiao2021@163.com (Y.M.); zhangpeng_cup@aliyun.com (P.Z.); curiosityguo2018@163.com (H.G.)

[2] Key Laboratory of Jiangxi Province for Persistent Pollutants Control and Resources Recycle, Nanchang Hangkong University, Nanchang 330063, China

* Correspondence: weiyc@cup.edu.cn

† These authors contributed equally to this work.

Abstract: Herein, we present an in-depth investigation into the enhancement of catalytic soot oxidation through cerium-doped three-dimensional ordered macroporous (3DOM) La-Co-Ni-based perovskites synthesized with the colloidal crystal template (CCT) method. The 3DOM structure significantly contributes to the accessibility and interaction efficiency between soot and catalyst. Based on the results of powder X-ray diffraction (XRD), N_2 adsorption-desorption measurements, scanning electron microscopy (SEM), temperature-programmed oxidation of NO (NO-TPO), temperature-programmed reduction of H_2 (H_2-TPR), in situ infrared Fourier transform spectroscopy (In-situ DRIFTS), and temperature-programmed oxidation (TPO) reactions, the role of cerium doping in modifying the structural and catalytic properties of 3DOM perovskite-type $La_{2-x}Ce_xCoNiO_6$ catalysts was investigated systematically. The optimized cerium doping ratio in $La_{2-x}Ce_xCoNiO_6$ catalysts can improve the microenvironment for efficient soot-catalyst contact, enhancing the catalytic activity of soot oxidation. Among the catalysts, the 3DOM $La_{0.8}Ce_{1.2}CoNiO_6$ catalyst shows the highest catalytic activity for soot oxidation, whose T_{10}, T_{50}, and T_{90} values are 306 °C, 356 °C, and 402 °C, respectively. The mechanism of the cerium doping effect for boosting soot oxidation is proposed: The doping of Ce ions can increase the surface oxygen species, which is the main active species for promoting the key step of NO oxidation to NO_2 in catalyzing soot oxidation. This research provides a new strategy to develop high-efficient non-noble metal catalysts for soot oxidation in pollution control and sustainable environmental practices.

Keywords: soot oxidation; 3DOM structure; $La_{2-x}Ce_xCoNiO_6$ catalysts; doping effect

Citation: Chen, K.; Xu, L.; Li, Y.; Xiong, J.; Han, D.; Ma, Y.; Zhang, P.; Guo, H.; Wei, Y. Cerium Doping Effect in 3DOM Perovskite-Type $La_{2-x}Ce_xCoNiO_6$ Catalysts for Boosting Soot Oxidation. *Catalysts* **2024**, *14*, 18. https://doi.org/10.3390/catal14010018

Academic Editor: Hamidreza Arandiyan

Received: 27 November 2023
Revised: 17 December 2023
Accepted: 24 December 2023
Published: 26 December 2023

1. Introduction

Soot particles, as a major component of particulate matter (PM), represent a significant air pollutant that poses serious threats to human health and the ecological environment [1,2]. In response, various countries have implemented stringent gas emission standards to control soot pollution [3]. Among the challenges in this area, reducing emissions from diesel engines, which represent the largest mobile source of soot, is significant for the environment [4]. A promising solution to reduce emissions involves the use of diesel particulate filters (CDPF) equipped with highly efficient catalysts [5]. The CDPF captures soot particles in the filter and subsequently oxidizes them with catalysts, thereby reducing PM exhaust into the atmosphere [6–8]. Effective oxidation of soot involves its complete conversion into carbon dioxide, which is a less harmful byproduct. However, this process requires temperatures (>500 °C) much higher than those in diesel engine exhausts (<400 °C) [9].

Therefore, developing catalysts that can effectively oxidize soot at lower temperatures is crucial, as it minimizes energy consumption and reduces the risk of filter damage due to high temperatures [10,11].

To date, researchers have effectively developed an array of diverse, highly efficient catalysts for deep catalytic soot oxidation at lower temperatures, encompassing noble metals [12–15], transition metal oxides [16–19], perovskite-type oxides [20–24], spinel-type oxides [25–27], rare-earth-based materials [28–30], and various other materials. Noble metal catalysts, characterized by their abundant unoccupied d-orbitals, demonstrate exceptional catalytic performance and have been commercially preferred for a long time [31,32]. However, due to the scarcity and high cost of noble metals, their usage is limited [33]. Preparing efficient non-Pt/Pd noble metal catalysts remains a challenge, yet it is not insurmountable [34,35]. As early as the 1970s, researchers such as Libby and Voorhoeve identified the high potential of Co-based catalysts and Mn-based catalysts for the purification of diesel engine exhaust [36,37]. With further research, perovskite-type catalysts have been tapped for catalytic properties that are no less than those of noble metal catalysts [38]. The team of J.H. Liu [22] has been able to reduce the T_{50} of the soot to 291 °C by doping K^+ to convert Mn^{3+} to Mn^{4+} to create more oxygen vacancies. X.L. Mei [39] successfully synthesized a series of non-noble metal perovskites with a three-dimensional ordered macropore (3DOM) structure by using the colloidal crystal template method. The 3DOM structure was used to increase the contact between catalyst and soot while changing the B-site atoms in perovskite to form the synergistic interaction of binary B-site ions. The research highlighted the practical application potential of 3DOM structural perovskite as a prominent non-noble metal nano-catalyst for the removal of diesel dust. The development of efficient and stable perovskite-type catalysts as alternatives to noble metal catalysts holds great significance for reducing soot particles in practical applications.

Catalytic soot combustion is a typical multi-phase catalytic reaction, occurring in the deep oxidation reaction of solid (soot)—solid (catalyst)—gas (O_2, NO_2); thereby necessitating higher requirements on the intrinsic redox capacity of the catalyst and the contact area between the catalyst and the soot particles [40,41]. Based on the characteristics of the soot oxidation reaction, two effective strategies can be derived for developing efficient catalysts: selecting substances with higher intrinsic catalytic activity and improving the contact efficiency of solid (soot) and solid (catalyst) [42]. The latter strategy is closely related to the microscopic morphology of the catalyst; for instance, the diameter of soot particles is generally greater than 25 nm, making it challenging to use the microporous (pore size less than 2 nm) and mesoporous (pore size between 2 nm and 50 nm) materials prepared by conventional methods [43]. However, the 3DOM structure synthesized via the CCT method features pore sizes exceeding 50 nm, which are advantageous for the mass transfer and diffusion of soot particles, thereby enhancing the contact efficiency between the soot and the catalyst [44].

Although the application of perovskite-type catalysts in catalyzing soot oxidation has been extensively explored, this includes strategies such as creating additional oxygen defects through alkali metal doping at the A-site to induce valence changes of transition metal ions at the B-site [45] and introducing multiple transition metal ions for a synergistic effect at the B-site [46]. However, it is seldom reported that the interaction resulting from doping variable-valent rare-earth metals at the A-site forms A-site variable-valent rare-earth metals in conjunction with B-site variable-valent transition metals. The results from both our preliminary experimental data and literature data showed that A-site doping with variable-valence rare earth metals positively impacts the performance of catalysts [47]. Therefore, doping variable-valence rare earth metals at the A-site of perovskite to enhance the catalytic activity in soot oxidation is a viable strategy.

In this study, we synthesized 3DOM perovskite-type $La_{2-x}Ce_xCoNiO_6$ catalysts by the CCT method. The 3DOM structure, characterized by its extensive porosity and high specific surface area, provides an abundance of active sites, thereby enhancing the catalytic effectiveness between soot particles and active sites. This structure also facilitates the

mass transfer and diffusion of soot and its oxidation products (CO and CO_2). Based on experimental data, Ce-doping La_2CoNiO_6 within a certain range is observed to enhance the catalytic activity for soot oxidation. Consequently, we propose a mechanism for the Ce-doping effect, where the incorporation of Ce ions augments the amount of surface oxygen species. In-situ DRIFTS results also indicate that this is a crucial step in promoting the oxidation of NO to NO_2, thereby significantly elevating the efficiency of soot catalytic oxidation. This work holds considerable significance for the design and construction of catalysts at the A-site of rare earth metal-doped perovskites.

2. Results and Discussions

2.1. Structural Properties

PMMA microspheres and 3DOM $La_{2-x}Ce_xCoNiO_6$ catalysts are illustrated in Figure 1. 3DOM catalysts are prepared by using three-dimensional close-packed PMMA microspheres (Figure 1A) as templates. As shown in Figure 1B–E, the perfect 3DOM structure can be seen in the orderly arrangement of macropores with a diameter of about 240 nm. The doping of Ce can affect the $La_{2-x}Ce_xCoNiO_6$ structure. As shown in Figure 1F, when x = 1.6 in $La_{2-x}Ce_xCoNiO_6$, it is difficult for the excessive Ce to be fully doped into the lattice of La_2CoNiO_6, and thus Ce will cover the catalyst surface as CeO_2. The accumulation of CeO_2 on the catalyst surface can seriously affect the structure and property of 3DOM La_2CoNiO_6 perovskite, which can interpret the catalytic activity of $La_{0.4}Ce_{1.6}CoNiO_6$ as the worst among $La_{2-x}Ce_xCoNiO_6$.

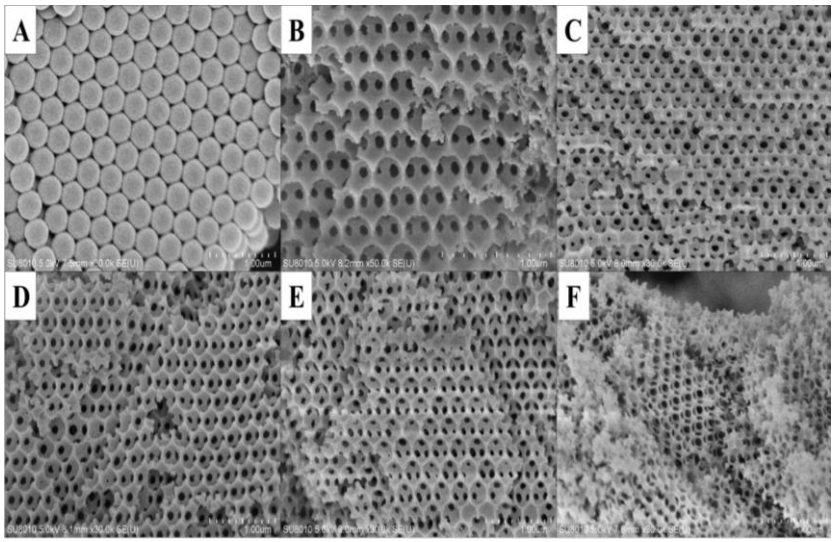

Figure 1. SEM images of PMMA microspheres and 3DOM $La_{2-x}Ce_xCoNiO_6$ catalysts: (**A**) PMMA microspheres; (**B**) La_2CoNiO_6; (**C**) $La_{1.6}Ce_{0.4}CoNiO_6$; (**D**) $La_{1.2}Ce_{0.8}CoNiO_6$; (**E**) $La_{0.8}Ce_{1.2}CoNiO_6$; (**F**) $La_{0.4}Ce_{1.6}CoNiO_6$.

To investigate the impact of Ce doping on the specific surface area of the catalyst, we conducted N_2 adsorption-desorption measurements and surface area analysis. As illustrated in Figure 2A, the BET isotherms exhibit type II isothermal adsorption characteristics and feature an H3-type hysteresis loop, which is indicative of pronounced macroporous structure adsorption characteristics. The marked increase in the adsorption amount of the samples at $P/P_0 > 0.8$ suggests that all samples possess a macroporous structure, and the Ce doping has no detrimental impact on the formation of the macroporous structure. With increasing Ce content, there is an observable expansion of the adsorption range from $P/P_0 > 0.8$ to $P/P_0 > 0.4$, which implies the emergence of small mesopores in the structure due to Ce doping. When the content ratio of La to Ce is 2:3, the hysteresis loop area reaches the maximum, which is consistent with the result that the specific surface area is the maximum. In Figure 2B, the size distribution of the porous structure for all 3DOM

$La_{2-x}Ce_xCoNiO_6$ catalysts is shown. 3DOM $La_{2-x}Ce_xCoNiO_6$ catalysts have a wide pore size distribution in the range of 3–10 nm.

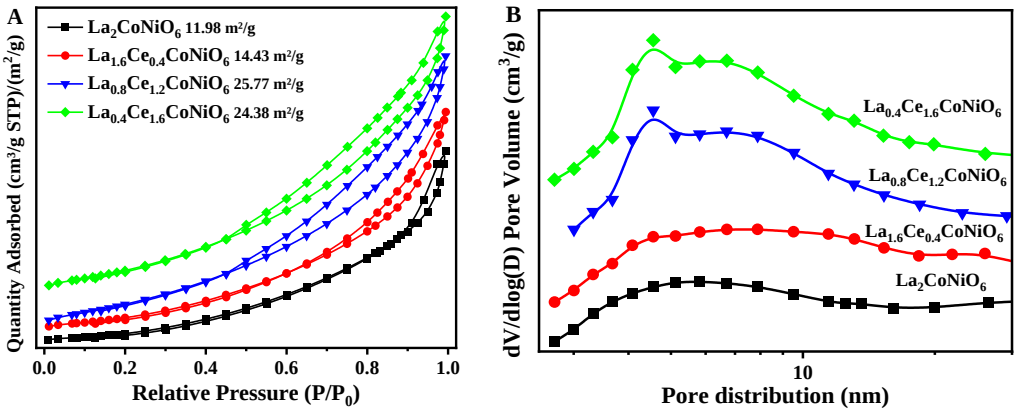

Figure 2. (**A**) N_2 adsorption-desorption isotherms and (**B**) pore size distribution curves of 3DOM $La_{2-x}Ce_xCoNiO_6$ catalysts.

Data from Table 1 also reveal that as the amount of cerium doping increases, the specific surface area of the catalyst progressively enlarges, reaching its maximum when the La:Ce ratio is 2:3. This suggests that the $La_{0.8}Ce_{1.2}CoNiO_6$ catalyst may possess more active sites for contact with soot. In conjunction with the soot-TPO data, this indeed could be one of the potential reasons for the enhanced activity. Moreover, with increasing Ce doping, the average pore size of the catalyst gradually decreases, indicating that excessive Ce might lead to pore blockage.

Table 1. Surface area, average pore volume, and average pore size of 3DOM $La_{2-x}Ce_xCoNiO_6$ catalysts.

3DOM Catalysts	S_{BET} (m^2/g)	Average Pore Volume (cm^3/g)	Average Pore Size (nm)
La_2CoNiO_6	12	0.07	9.2
$La_{1.6}Ce_{0.4}CoNiO_6$	16	0.08	8.8
$La_{0.8}Ce_{1.2}CoNiO_6$	26	0.10	7.7
$La_{0.4}Ce_{1.6}CoNiO_6$	24	0.11	7.6

In order to explore the structural effects of Ce doping on La-Co-Ni-based perovskites (PDF#97-015-0874), we characterized the samples by XRD analysis. Examination of the X-ray diffraction (XRD) spectra for a diverse array of samples, as illustrated in Figure 3, reveals a notable trend in the $La_{2-x}Ce_xCoNiO_6$ perovskite system. Specifically, in cases where cerium doping in $La_{2-x}Ce_xCoNiO_6$ perovskite is characterized by $x \leq 1.2$, a discernible shift of the principal diffraction peak of La_2CoNiO_6 perovskite, typically observed at 33.2°, is evident. This peak is observed to gradually transition towards lower angles in comparison to its position in La_2CoNiO_6 (undoped) and $La_{2-x}Ce_xCoNiO_6$ (cerium-doped variants). This shift underscores the structural modifications induced by varying cerium concentrations within the perovskite matrix. It can be inferred that the cerium element is doping. La_2CoNiO_6 perovskite and $La_{2-x}Ce_xCoNiO_6$ perovskite are formed. With the increase in cerium content, there is a noticeable increase in the CeO_2 peak at 28.0°, which gradually moves to the right, indicative of an increase in cerium content. When x reaches 1.6, the peak at 28.0° reverts to the maximum characteristic peak of CeO_2, and the maximum characteristic peak of La_2CoNiO_6 perovskite at 32.8° and 33.2° is significantly weakened, suggesting that the cubic fluorite structure of CeO_2 predominates at this time and the perovskite structure is basically lost. An excessive amount of cerium dioxide might lead to the possibility that the active sites have been covered by cerium dioxide. The catalytic performance of CeO_2 for soot is unsatisfactory, resulting in a sharp decrease in activity observed here, which is consistent with the soot-TPO data.

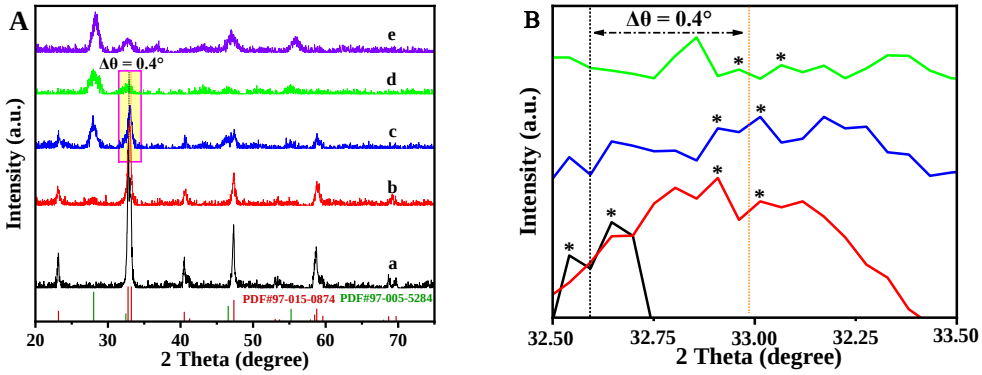

Figure 3. (**A**) XRD results of 3DOM $La_{2-x}Ce_xCoNiO_6$ catalysts. (**B**) Partially enlarged view of the diffraction peak yellow area of A. (a) La_2CoNiO_6; (b) $La_{1.6}Ce_{0.4}CoNiO_6$; (c) $La_{1.2}Ce_{0.8}CoNiO_6$; (d) $La_{0.8}Ce_{1.2}CoNiO_6$; (e) $La_{0.4}Ce_{1.6}CoNiO_6$. * represents the characteristic peaks of each XRD image.

2.2. Catalytic Activity Performance

Under the condition of loose contact between catalyst and soot (mass ratio 10:1), the results of soot-TPO are presented in Figure 4 and Table 2. Under identical test conditions, the T_{10}, T_{50}, T_{90}, and $S_{CO2}{}^m$ values for soot oxidation without catalyst are measured to be 487 °C, 599 °C, 651 °C, and 30.45%, respectively. In Table 1, it is evident that both 3DOM $LaNiO_3$ and 3DOM $LaCoO_3$, both lanthanum-based perovskites, demonstrate excellent catalytic performance for soot oxidation. Additionally, 3DOM La_2CoNiO_6 double-perovskite, resulting from the doping of Co and Ni elements in equal amounts at the B site of the perovskite, exhibits improved catalytic performance compared to 3DOM $LaNiO_3$ and 3DOM $LaCoO_3$. The T_{10}, T_{50}, T_{90}, and $S_{CO2}{}^m$ values of the 3DOM La_2CoNiO_6 catalyst for soot oxidation are 311 °C, 400 °C, 439 °C, and 99.64%, respectively. As illustrated in Figure 4 and Table 1, when the lanthanum-cerium molar ratio is less than 2:3 (i.e., $x \leq 1.2$ in $La_{2-x}Ce_xCoNiO_6$), the catalytic performance of the 3DOM $La_{2-x}Ce_xCoNiO_6$ catalyst for soot oxidation is enhanced with the increase of cerium doping in the 3DOM La_2CoNiO_6 crystal lattice. Among them, the 3DOM $La_{0.8}Ce_{1.2}CoNiO_6$ catalyst shows the best catalytic performance, and its T_{10}, T_{50}, T_{90}, and $S_{CO2}{}^m$ values are 306 °C, 356 °C, 402 °C, and 99.80%, respectively. This may be attributed to the increase in the number of active oxygen species on the surface induced by Ce doping [48], which promotes the oxidation of NO to NO_2. However, when the lanthanum-cerium molar ratio exceeds 2:3 (i.e., $x \geq 1.2$ in $La_{2-x}Ce_xCoNiO_6$), not all of the Ce ions can enter the lattice, and a portion of Ce ions will cover the surface of the 3DOM $La_{2-x}Ce_xCoNiO_6$ catalyst in the form of CeO_2 oxides. This is the main reason for the obvious decrease in the catalytic performance of 3DOM $La_{2-x}Ce_xCoNiO_6$ ($x \geq 1.2$ in $La_{2-x}Ce_xCoNiO_6$).

Table 2. Catalytic activity and CO_2 selectivity of 3DOM $La_{2-x}Ce_xCoNiO_6$ catalysts for soot oxidation under loose contact.

3DOM Catalysts	T_{10} (°C)	T_{50} (°C)	T_{90} (°C)	$S_{CO2}{}^m$ (%)
La_2CoNiO_6	331	400	439	99.64
$La_{1.9}Ce_{0.1}CoNiO_6$	318	388	437	99.99
$La_{1.6}Ce_{0.4}CoNiO_6$	311	372	420	99.75
$La_{1.2}Ce_{0.8}CoNiO_6$	312	363	413	99.67
$La_1Ce_1Co_1Ni_1O_6$	303	361	404	99.86
$La_{0.8}Ce_{1.2}CoNiO_6$	306	356	402	99.80
$La_{0.4}Ce_{1.6}CoNiO_6$	348	414	452	98.73
$LaCoO_3$	345	427	468	97.21
$LaNiO_3$	364	437	486	97.90
soot (no catalyst)	487	599	651	30.45

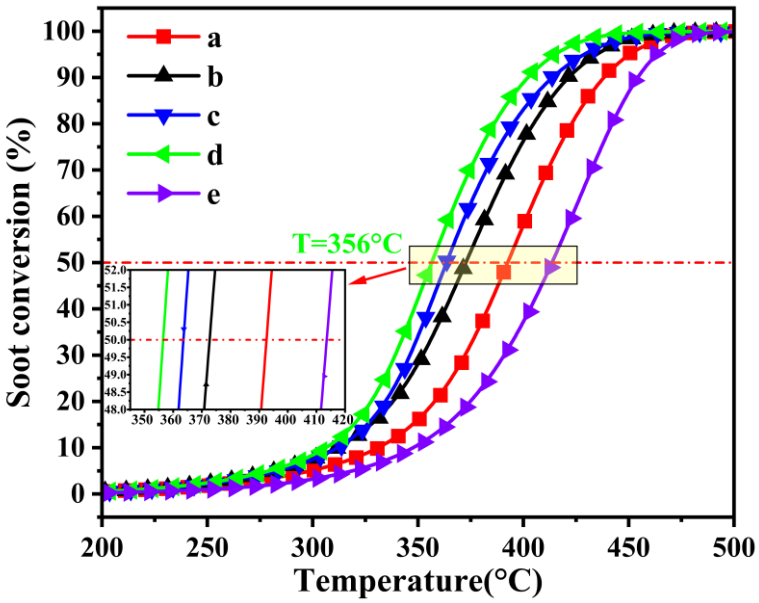

Figure 4. Soot conversion percentage results of 3DOM $La_{2-x}Ce_xCoNiO_6$ catalysts: (a) La_2CoNiO_6; (b) $La_{1.6}Ce_{0.4}CoNiO_6$; (c) $La_{1.2}Ce_{0.8}CoNiO_6$; (d) $La_{0.8}Ce_{1.2}CoNiO_6$; (e) $La_{0.4}Ce_{1.6}CoNiO_6$.

According to Figure 5, the cycling stability of soot-TPO was tested under the conditions of an optimal cerium doping ratio ($La_{0.8}Ce_{1.2}CoNiO_6$ catalyst). The results indicate that, within the permissible margin of error, the catalyst maintains consistently high catalytic activity in terms of soot conversion rate and selectivity towards carbon dioxide. The long-term efficacy of the catalyst is robustly demonstrated.

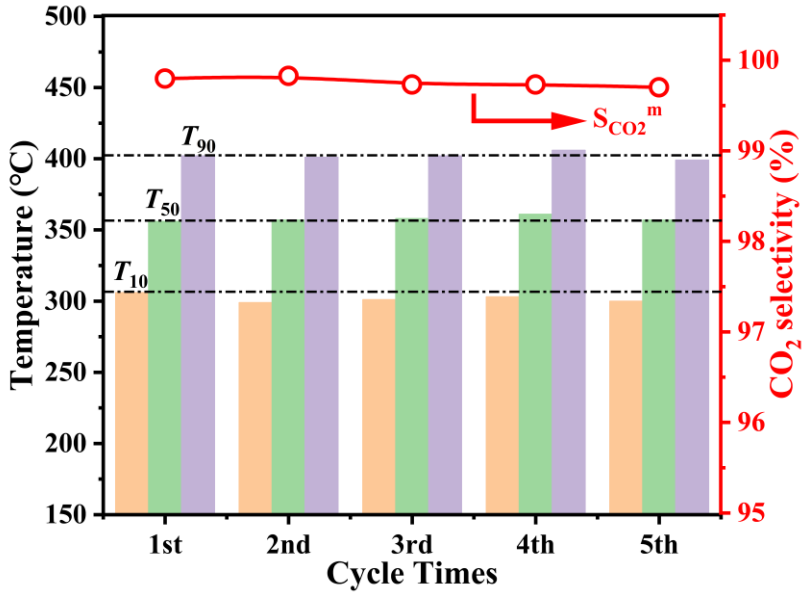

Figure 5. Stability test results of the 3DOM $La_{0.8}Ce_{1.2}CoNiO_6$ catalyst.

2.3. H_2-TPR Profiles

The redox capacity of the catalyst, as one of the key parameters for the catalytic oxidation of soot, deserves to be explored, so the H_2-TPR test is used to investigate the redox properties of the catalyst. In Figure 6, the peak in the α region should be attributed to the reduction of active oxygen species on the catalyst surface [49,50]. With the increase of Ce doping in 3DOM $La_{2-x}Ce_xCoNiO_6$, we can see that the peak-up temperatures in the α-region are 127 °C, 118 °C, 60 °C, and 109 °C, respectively. The lowest peak-up

temperature (60 °C) of the active oxygen reduction peak is observed when the La to Ce molar ratio is 2:3. This may be due to the substitution of La by Ce, which causes lattice oxygen migration and conversion, resulting in an increase in adsorbed oxygen on the surface [51]. In Figure 6, the peaks at β are the result of the reduction of Ni^{3+} to Ni^{2+}, and the peaks at γ are the result of the reduction of Co^{2+} to Co [39,52]. With the increase in Ce doping, the reduction peaks at both β and γ are shifted to lower temperatures, which may be attributed to the interaction among Ni, Co, and Ce. And the interaction can weaken the M-O (M = Ni, Co), which may also be the reason for the lower peak-up temperature in the α-region.

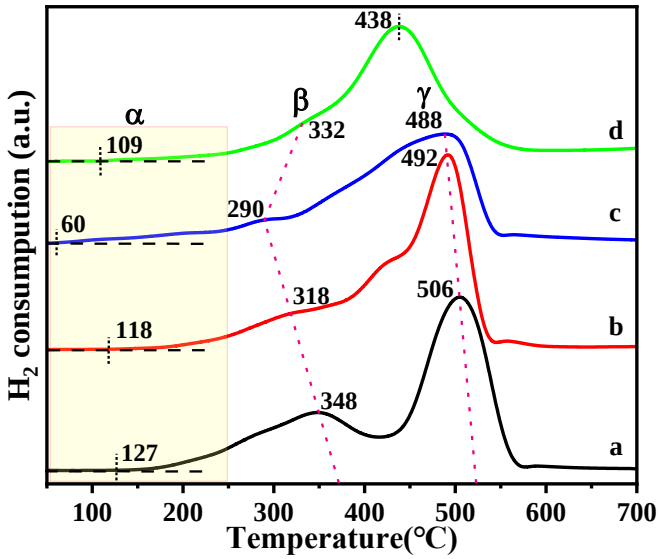

Figure 6. H_2-TPR profiles of 3DOM $La_{2-x}Ce_xCoNiO_6$ catalysts: (a) La_2CoNiO_6; (b) $La_{1.6}Ce_{0.4}CoNiO_6$; (c) $La_{0.8}Ce_{1.2}CoNiO_6$; (d) $La_{0.4}Ce_{1.6}CoNiO_6$.

Among the H_2 consumption curves of all catalysts, the 3DOM $La_{0.8}Ce_{1.2}CoNiO_6$ catalyst exhibits the lowest temperatures of the reduction peaks located at β (290 °C) and γ (480 °C), which indicates that the strongest interaction among Ce, Ni, and Co is observed for the 3DOM $La_{0.8}Ce_{1.2}CoNiO_6$ catalyst. It also shows the lowest peak-up temperature of active oxygen species in the α-region (60 °C), which may predict the best redox capacity of the 3DOM $La_{2-x}Ce_xCoNiO_6$ catalyst, which also coincides with the data of soot-TPO. In the H_2 consumption curve of $La_{0.4}Ce_{1.6}CoNiO_6$, the peak at β is shifted to higher temperatures, the peak at γ disappears, and a reduction peak of CeO_2 appears at 438 °C. It may be due to the formation of the Ce-Ce interaction by doping excess Ce, which weakens Ce-Ni, causing the peak at β to shift to a higher temperature. And the excess CeO_2 can encapsulate Co, making the Co^{2+} reduction peak disappear, which is consistent with the fact that the characteristic peaks of Co-related species are not detected in the XRD of $La_{0.4}Ce_{1.6}CoNiO_6$.

2.4. NO-TPO Measurement

It is well known that the NO_2-assisted mechanism plays a pivotal role in catalytic soot oxidation. The NO_2 generated by the rapid oxidation of NO in the engine exhaust gas is a highly efficient mobile oxidizing species. Owing to the strong oxidizing ability of NO_2, it can easily oxidize the soot particles when it comes into contact with them.

As shown in Figure 7, the NO activation temperatures of La_2CoNiO_6, $La_{1.6}Ce_{0.4}CoNiO_6$, $La_{0.8}Ce_{1.2}CoNiO_6$, and $La_{0.4}Ce_{1.6}CoNiO_6$ catalysts are 322, 319, 312, and 355 °C, respectively. It can be found that with the increase of Ce ions doped into the La_2CoNiO_6 perovskite lattice, the activation ability of the catalyst for NO becomes stronger and then weaker. And the $La_{0.8}Ce_{1.2}CoNiO_6$ catalyst can exhibit the lowest NO activation temperature and the maximum NO_2 concentration. This enhancement is attributed to the doping of Ce ions,

which induces the creation of more oxygen vacancies in the La_2CoNiO_6 catalyst, thereby enhancing its adsorption-activation capacity for gaseous reactants (O_2 and NO). However, the overdoping of Ce ions can destroy the structure of $La_{2-x}Ce_xCoNiO_6$ perovskite. As shown in the XRD results (Figure 3), the $La_{0.4}Ce_{1.6}CoNiO6$ catalyst shows an extremely obvious characteristic peak of CeO_2 at around 28°, and the characteristic peak of $La_{2-x}Ce_xCoNiO_6$ perovskite at around 33° weakens, which indicates that the main bulk of the catalyst is likely to have changed from $La_{2-x}Ce_xCoNiO_6$ to CeO_2. Consequently, the $La_{0.4}Ce_{1.6}CoNiO_6$ catalyst shows the worst NO oxidizing ability of the Ce-doped $La_xCe_{2-x}CoNiO_6$ catalysts, and its catalytic activity for soot oxidation is also the worst.

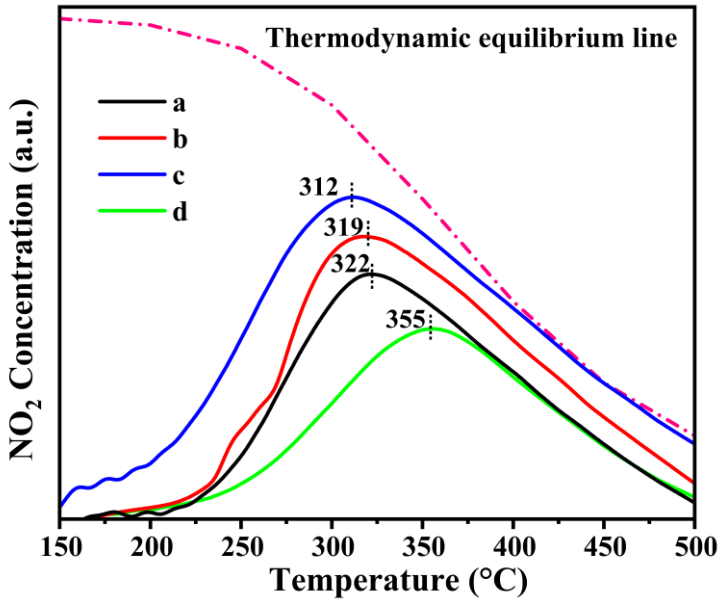

Figure 7. NO-TPO results of 3DOM $La_{2-x}Ce_xCoNiO_6$ catalysts: (a) La_2CoNiO_6; (b) $La_{1.6}Ce_{0.4}CoNiO_6$; (c) $La_{0.8}Ce_{1.2}CoNiO_6$; (d) $La_{0.4}Ce_{1.6}CoNiO_6$.

2.5. NO Oxidation In-Situ DRIFTS

Previous studies indicate that the presence of nitrogen dioxide is conducive to the deep oxidation of soot. To explore the surface intermediates formed during the oxidation process of NO in cerium-doped La_2CoNiO_6, the in-situ DRIFTS tests were conducted with a temperature gradient of 50 °C between 50 °C and 450 °C. As illustrated in Figure 8, at a lower temperature (50 °C), the following compounds are present on the catalyst surface in $La_{0.8}Ce_{1.2}CoNiO_6$ perovskite: N-O deformation vibration (at 837 cm^{-1}) [53,54], Symmetrically adsorbed NO at the edge and hollow position around the Ce element (at 1150 cm^{-1}) [55], nitrite asymmetric vibration (at 1215 cm^{-1}) [56], bridging NO_3^- (at 1245 cm^{-1}) [57], NO_2 adsorbed—at transition metal ion surface (at 1337 cm^{-1}) [58]; N_2O_5 (at 1415 cm^{-1}) [59]; and bidentate nitrates (at 1560 cm^{-1}) [60,61]. An increase in temperature results in an intensified four characteristic peaks at 1215 cm^{-1}, 1245 cm^{-1}, 1337 cm^{-1}, and 1415 cm^{-1}. This peak gradually diminishes and evolves into a new peak at 1377 cm^{-1}, suggesting the transformation of nitrite and certain NO_x compounds into nitrate ions with a D_{3h} symmetric structure (at 1377 cm^{-1}) [62]. According to the literature, at temperatures above 350 °C, nitrate ions gradually decompose into gaseous nitrogen dioxide. Literature indicates that at temperatures above 350 °C, nitrate ions tend to decompose into gaseous nitrogen dioxide. As the reactant gas stream reaches the soot surface, it facilitates the oxidation of soot to carbon dioxide. However, with increasing temperature, the peak at 1377 cm^{-1} continues to intensify, while the intensity of the surrounding peaks diminishes. The increasing amount of nitrate ions with temperature suggests that these ions at this location are the key products of the NO oxidation process.

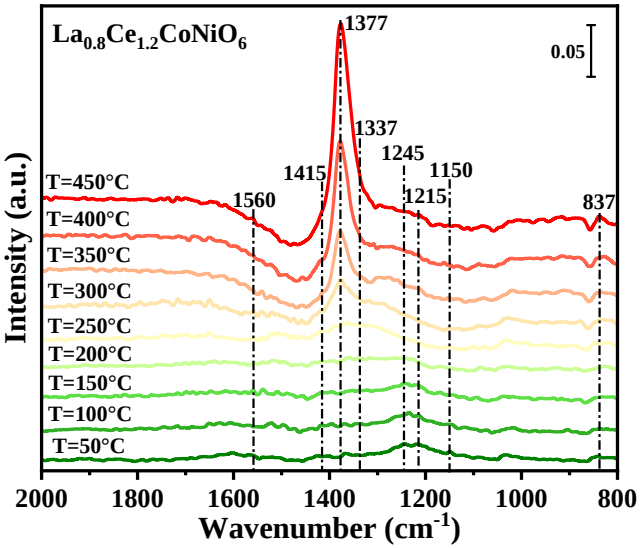

Figure 8. NO oxidation in-situ DRIFTS results of the 3DOM $La_{0.8}Ce_{1.2}CoNiO_6$ catalyst.

3. Experimental Sections

3.1. Materials

Ethylene glycol, Methanol, Lanthanum nitrate ($La(NO_3)_3{\cdot}6H_2O$), and cobalt nitrate ($Co(NO_3)_2{\cdot}6H_2O$) were obtained from Shanghai Aladdin Biochemical Technology Co., Ltd. (Shanghai, China). Cerium nitrate ($Ce(NO_3)_3{\cdot}6H_2O$) was purchased from Beijing Bailingwei Technology Co., Ltd. (Beijing, China). Nickel nitrate was bought from Shandong Aex Chemical Technology Co., Ltd. (Weifang, Shandong, China). Methyl methacrylate (MMA) was obtained from Shanghai Macklin Biochemical Co., Ltd. (Shanghai, China).

3.2. Preparation Methods

3.2.1. Preparation of Polymethyl Methacrylate (PMMA) Microsphere Template

A classic soap-free emulsion polymerization technique was employed to synthesize polymethyl methacrylate (PMMA) microspheres, which served as a template for subsequent preparations. Initially, 500 mL of deionized water and 120 mL of methyl methacrylate (MMA) were introduced into a four-necked flask; an electric stirring paddle and a condenser tube were assembled, followed by the introduction of nitrogen gas at a flow rate of 50 mL/min into the reaction vessel as a protective atmosphere. Upon heating the mixture to 80 °C, 0.6 g of refined potassium persulfate (KPS) was added as the reaction initiator, and the solution was stirred at 350 rpm and 80 °C for 1.5 h. Following the completion of the reaction, the mixture was first removed and then filtered. Subsequently, it was centrifuged at 300 rpm for 12 h and finally dried to obtain close-packed PMMA microspheres suitable for use as templates.

3.2.2. Syntheses of 3DOM $La_{2-x}Ce_xCoNiO_6$ Catalysts

The colloidal crystal template (CCT) method is employed to synthesize 3DOM $La_{2-x}Ce_xCoNiO_6$ perovskite materials, utilizing a specified ratio of lanthanum, cerium, cobalt, and nickel nitrate solutions in ethylene glycol and methanol (ethylene glycol:methanol = 3:2). Citric acid is added at a molar ratio equal to half of the total metal ions, serving as a complexing agent. Once fully dissolved, the solution is subjected to magnetic stirring at 250 rpm for 2 h at room temperature to ensure complete complexation. Following complexation, a suitable quantity of the prepared PMMA microspheres is added, and the mixture is maintained at 40 °C under −0.8 Bar vacuum for 12 h, allowing the solution to fully infiltrate the gaps within the templates. After filtration until near-dryness, the material is crystallized in a 60 °C oven for 8 h, then removed and subjected to a controlled temperature increase in

a tube furnace to eliminate the PMMA template, ultimately yielding the 3DOM structure of perovskite.

3.3. Catalysts Characterization

The detailed characterizations about the physicochemical properties of the prepared catalysts, such as powder X-ray diffraction (XRD), N_2 adsorption-desorption measurements, scanning electron microscopy (SEM), temperature-programmed oxidation of NO (NO-TPO), temperature-programmed reduction of H_2 (H_2-TPR), and in situ infrared Fourier transform spectroscopy (In-situ DRIFTS), are as follows:

The structural and physical phases were investigated by a powder X-ray diffraction (XRD) spectrometer (Bruker D8 Advance) with Cu Kα radiation (λ = 1.54184 Å) from 5 to 90° with a scanning rate of 4° min^{-1}. N_2 adsorption-desorption experiments were operated on a Micromeritics TriStar-II 3020 instrument. Scanning electron microscopic (SEM) images were obtained on a Quanta 200F instrument using accelerating voltages of 5 kV. The temperature-programmed reduction of hydrogen (H_2-TPR) was carried out on the HUASI DAS-7200 instrument. In situ diffuse reflectance infrared Fourier transform spectra (In situ DRIFTS) experiments were recorded using a SHIMADZU IRTracer-100 infrared spectrometer over a range of 4000–400 cm^{-1}.

3.4. Evaluation of Catalytic Activity

Temperature-Programmed Co-Oxidation of Soot (Soot-TPO)

The catalytic activity for soot oxidation is evaluated by a temperature-programmed oxidation (TPO) reaction using Printex-U (Degussa, Germany, diameter ~ 25 nm) as model soot particles. The TPO reaction ranges from 150 to 700 °C at a ramping rate of 2 °C min^{-1}. The catalyst (100 mg) and soot particle (10 mg) are mixed into the loose contact mode by using a spoon in order to simulate the actual conditions of catalytic soot purification. The flow rate of gaseous reactants is 50 mL min^{-1} containing O_2 (5 vol%), NO (0.1 vol%), and N_2. The outlet gas products are analyzed by an online gas chromatograph (GC 9890B, Shanghai, China) with an FID detector. The catalytic performance is evaluated by the T_{10}, T_{50}, and T_{90} values, which are defined as the temperatures at 10%, 50%, and 90% soot conversions, respectively. The CO_2 selectivity (S_{CO2}) of oxidation is defined as the CO_2 outlet concentration divided by the sum of the CO_2 and CO outlet concentrations.

4. Conclusions

Preparation of three-dimensional ordered macroporous (3DOM) Perovskite-type $La_{2-x}Ce_xCoNiO_6$ catalysts with different Ce doping by the CCT method can represent a significant advance in the field of environmental catalysis, particularly in the context of soot oxidation in diesel exhaust systems. The unique three-dimensional ordered macroporous structure of the synthesized perovskites crystals is conducive to raising contact with soot particles, thus leading to improved oxidation rates. By optimizing the cerium doping ratio in La-Co-Ni-based perovskite catalysts, the active oxygen concentration on the catalyst surface is enhanced. As a result, the catalytic efficiency is significantly raised at lower temperatures, which is a critical need in pollution control technology. This research not only contributes to the development of non-noble metal catalysts but also opens avenues for further exploration in the design and application of cost-effective and environmentally benign catalysts. The implications of our work extend beyond the realm of diesel particulate reduction, offering potential solutions to a broader range of environmental challenges. Future research will focus on scaling these findings for industrial applications and exploring the long-term stability and effectiveness of these catalysts under real-world conditions.

Author Contributions: Methodology, K.C., L.X. and Y.M.; Formal analysis, D.H.; Investigation, K.C., Y.L., J.X., P.Z., H.G. and Y.W.; Data curation, L.X.; Writing—original draft, K.C. and L.X.; Visualization, K.C.; Funding acquisition, Y.W. All authors have read and agreed to the published version of the manuscript.

Funding: This work was supported by the National Key Research and Development Program of China (2022YFB3504100, 2022YFB3506200), the National Natural Science Foundation of China (22376217, 22208373), and the Beijing Nova Program (20220484215).

Data Availability Statement: Data are contained within this article.

Conflicts of Interest: The authors declare no conflicts of interest.

References

1. Guan, B.; Zhan, R.; Lin, H.; Huang, Z. Review of the state-of-the-art of exhaust particulate filter technology in internal combustion engines. *J. Environ. Manag.* **2015**, *154*, 225–258. [CrossRef] [PubMed]
2. Fayyazbakhsh, A.; Bell, M.L.; Zhu, X.; Mei, X.; Koutný, M.; Hajinajaf, N.; Zhang, Y. Engine emissions with air pollutants and greenhouse gases and their control technologies. *J. Clean. Prod.* **2022**, *376*, 134260. [CrossRef]
3. Lou, D.; Xiang, B.; Zhang, Y.; Fang, L.; Tan, P.; Hu, Z. Study on the Catalytic Characteristics of Noble Metal Catalysts with Different Pt/Pd Ratios for Soot Combustion. *ACS Omega* **2023**, *8*, 20834–20844. [CrossRef] [PubMed]
4. Kozak, M.; Merkisz, J. Oxygenated Diesel Fuels and Their Effect on PM Emissions. *Appl. Sci.* **2022**, *12*, 7709. [CrossRef]
5. Weng, R.; Mei, X.; Zhang, Z.; Xin, Y.; Xu, J.; Zhang, Y.; Zhang, J. Affecting factors of electrified soot combustion on potassium-supported antimony tin oxides. *Chem. Eng. J.* **2023**, *465*, 143046. [CrossRef]
6. Feng, Q.; Lou, D.M.; Tan, P.Q.; Hu, Z.Y.; Cui, J.G. Effect of catalyzed diesel particulate filter on gaseous emissions from automobile diesel engine. *J. Fuel Chem. Technol.* **2014**, *42*, 1513–1521.
7. Zhang, Y.-H.; Lou, D.-M.; Tan, P.-Q.; Hu, Z.-Y. Effects of DOC+CDPF on Emission Characteristics of Heavy-duty Diesel Vehicle. *Huan Jing Ke Xue* **2017**, *38*, 1828–1834. [CrossRef] [PubMed]
8. Zhang, Y.; Lou, D.; Tan, P.; Hu, Z.; Fang, L. Effect of catalyzed diesel particulate filter and its catalyst loading on emission characteristics of a non-road diesel engine. *J. Environ. Sci.* **2023**, *126*, 794–805. [CrossRef]
9. Shi, Q.; Liu, T.; Li, Q.; Xin, Y.; Lu, X.; Tang, W.; Zhang, Z.; Gao, P.-X.; Anderson, J.A. Multiple strategies to decrease ignition temperature for soot combustion on ultrathin MnO_{2-x} nanosheet array. *Appl. Catal. B* **2019**, *246*, 312–321. [CrossRef]
10. Yang, Z.; Zhang, N.; Xu, H.; Li, Y.; Ren, L.; Liao, Y.; Chen, Y. Boosting diesel soot catalytic combustion via enhancement of solid(catalyst)-solid(soot) contact by tailoring micrometer scaled sheet-type agglomerations of CeO_2-ZrO_2 catalyst. *Combust. Flame* **2022**, *235*, 111700. [CrossRef]
11. Mei, X.; Zhu, X.; Zhang, Y.; Zhang, Z.; Zhong, Z.; Xin, Y.; Zhang, J. Decreasing the catalytic ignition temperature of diesel soot using electrified conductive oxide catalysts. *Nat. Catal.* **2021**, *4*, 1002–1011. [CrossRef]
12. Li, Y.; Guo, H.; Xiong, J.; Ma, Y.; Li, X.; Zhang, P.; Zhang, S.; Wei, Y. The Catalyst of Ruthenium Nanoparticles Decorated Silicalite-1 Zeolite for Boosting Catalytic Soot Oxidation. *Catalysts* **2023**, *13*, 1167. [CrossRef]
13. Li, Y.; Qin, T.; Wei, Y.; Xiong, J.; Zhang, P.; Lai, K.; Chi, H.; Liu, X.; Chen, L.; Yu, X.; et al. A single site ruthenium catalyst for robust soot oxidation without platinum or palladium. *Nat. Commun.* **2023**, *14*, 7149. [CrossRef] [PubMed]
14. Lee, J.H.; Jo, D.Y.; Choung, J.W.; Kim, C.H.; Ham, H.C.; Lee, K.-Y. Roles of noble metals (M = Ag, Au, Pd, Pt and Rh) on CeO_2 in enhancing activity toward soot oxidation: Active oxygen species and DFT calculations. *J. Hazard. Mater.* **2021**, *403*, 124085. [CrossRef] [PubMed]
15. He, L.; Zhang, Y.; Zang, Y.; Liu, C.; Wang, W.; Han, R.; Ji, N.; Zhang, S.; Liu, Q. Promotion of A-Site Ag-Doped Perovskites for the Catalytic Oxidation of Soot: Synergistic Catalytic Effect of Dual Active Sites. *ACS Catal.* **2021**, *11*, 14224–14236. [CrossRef]
16. Li, C.; Li, R.; Wang, Y.; Niu, R.; Guo, Q.; Zhang, C. Transition metal modified manganese-based catalysts for soot oxidation promoted by noncompetitive adsorption of oxygen: Experiments and DFT calculations. *J. Ind. Eng. Chem.* **2023**, *126*, 454–464. [CrossRef]
17. Portillo-Vélez, N.S.; Zanella, R. Comparative study of transition metal (Mn, Fe or Co) catalysts supported on titania: Effect of Au nanoparticles addition towards CO oxidation and soot combustion reactions. *Chem. Eng. J.* **2020**, *385*, 123848. [CrossRef]
18. Zhu, Y.; Chen, Z.; Li, H.; Wang, Q.; Liu, X.; Hu, Y.; Su, C.; Duan, R.; Chen, S.; Lan, L. Effect of oxygen vacancy and highly dispersed MnO_x on soot combustion in cerium manganese catalyst. *Sci. Rep.* **2023**, *13*, 3386. [CrossRef]
19. Cao, C.; Yang, H.; Xiao, J.; Yang, X.; Ren, B.; Xu, L.; Liu, G.; Li, X. Catalytic diesel soot elimination over potassium promoted transition metal oxide (Co/Mn/Fe) nanosheets monolithic catalysts. *Fuel* **2021**, *305*, 121446. [CrossRef]
20. Wei, K.; Wang, X.; Shi, L.; Yang, S.; Xue, Z.; Qin, W.; Wang, J.; Xu, K.; Zhang, X. Potassium promoted Fe–Ce composite oxides monolithic catalysts for catalytic soot combustion. *Chem. Pap.* **2023**, *77*, 7045–7052. [CrossRef]
21. Wang, M.; Han, Z.; Liu, Y.; Gao, C.; Pan, X.; Zhou, S. The influence of partial substitution of Ce with K in $CeMO_3$ (M = Mn, Fe, Co, Ni, Cu) perovskite catalysts on soot combustion performance. *J. Environ. Chem. Eng* **2023**, *11*, 110850. [CrossRef]
22. Liu, J.; Wang, Y.; Sun, P.; Wang, P.; Zhang, C.; Ma, H. Experimental and theoretical study on $La_{0.5}K_{0.5}Mn_{1-x}Fe_xO_3$ perovskite catalysts for mild temperature soot combustion and simultaneous removal of soot and NO. *Fuel Process. Technol.* **2023**, *246*, 107760. [CrossRef]
23. Montilla-Verdú, S.; Torregrosa-Rivero, V.; Díaz-Verde, A.; Illán-Gómez, M.J. $BaFe_{1-x}Ni_xO_3$ Catalysts for NO_x-Assisted Diesel Soot Oxidation. *Top. Catal.* **2023**, *66*, 839–849. [CrossRef]

24. Yu, X.; Yu, D.; Wang, L.; Ren, Y.; Chen, M.; Fan, X.; Zhao, Z.; Sojka, Z.; Kotarba, A.; Wei, Y.; et al. Ultralight and spongy La–Mn-based perovskite catalysts modified by alkali metals and Ce: Facile synthesis and excellent catalytic performance for soot combustion. *Catal. Sci. Technol.* **2023**, *13*, 1208–1220. [CrossRef]
25. Zhang, F.; Zhu, X.; Wu, H.; Wu, X.; Zhou, Z.; Chen, G.; Yang, G. Activity and Stability of Cu-Based Spinel-Type Complex Oxides for Diesel Soot Combustion. *ChemistrySelect* **2021**, *6*, 14019–14026. [CrossRef]
26. Chen, H.; Li, T.; Xu, Z.; Wang, W.; Wang, H. Oxidation of soot promoted by Fe-based spinel catalysts. *Mater. Res. Express* **2022**, *9*, 015502. [CrossRef]
27. Zhang, S.; Zhu, X.; Zheng, C.; Hu, D.; Zhang, J.; Gao, X. Study on Catalytic Soot Oxidation over Spinel Type ACo_2O_4 (A = Co, Ni, Cu, Zn) Catalysts. *Aerosol Air Qual. Res.* **2017**, *17*, 2317–2327. [CrossRef]
28. Tsai, Y.-C.; Kwon, E.; Park, Y.-K.; Nhat Huy, N.; Lisak, G.; Hsu, P.-S.; Hu, C.; Lin, K.-Y.A. Broccoli-like CeO_2 with Hierarchical/Porous Structures, and promoted oxygen vacancy as an enhanced catalyst for catalytic diesel soot elimination. *Sep. Purif. Technol.* **2022**, *281*, 119867. [CrossRef]
29. Alcalde-Santiago, V.; Davó-Quiñonero, A.; Lozano-Castelló, D.; Bueno-López, A. On the soot combustion mechanism using 3DOM ceria catalysts. *Appl. Catal. B* **2018**, *234*, 187–197. [CrossRef]
30. Woźniak, P.; Małecka, M.A.; Chinchilla, L.; Trasobares, S. 3D hierarchically structured $Ce_{1-x}Gd_xO_{2-x/2}$ mixed oxide particles: The role of microstructure, porosity and multi-level architecture stability in soot and propane oxidation. *Mater. Res. Bull.* **2022**, *151*, 111816. [CrossRef]
31. Kim, J.H.; Shin, D.; Lee, J.; Baek, D.S.; Shin, T.J.; Kim, Y.-T.; Jeong, H.Y.; Kwak, J.H.; Kim, H.; Joo, S.H. A General Strategy to Atomically Dispersed Noble Metal Catalysts for Unravelling Their Catalytic Trends for Oxygen Reduction Reaction. *ACS Nano* **2020**, *14*, 1990–2001. [CrossRef] [PubMed]
32. Giménez-Mañogil, J.; Quiles-Díaz, S.; Guillén-Hurtado, N.; García-García, A. Catalyzed Particulate Filter Regeneration by Platinum Versus Noble Metal-Free Catalysts: From Principles to Real Application. *Top. Catal.* **2017**, *60*, 2–12. [CrossRef]
33. Zhang, X.; Liu, Y.; Deng, J.; Zhao, X.; Zhang, K.; Yang, J.; Han, Z.; Jiang, X.; Dai, H. Three-dimensionally ordered macroporous $Cr_2O_3-CeO_2$: High-performance catalysts for the oxidative removal of trichloroethylene. *Catal. Today* **2020**, *339*, 200–209. [CrossRef]
34. Ren, W.; Ding, T.; Yang, Y.; Xing, L.; Cheng, Q.; Zhao, D.; Zhang, Z.; Li, Q.; Zhang, J.; Zheng, L.; et al. Identifying Oxygen Activation/Oxidation Sites for Efficient Soot Combustion over Silver Catalysts Interacted with Nanoflower-Like Hydrotalcite-Derived CoAlO Metal Oxides. *ACS Catal.* **2019**, *9*, 8772–8784. [CrossRef]
35. Qi, B.; Li, Z.; Lou, D.; Zhang, Y. Experimental investigation on the effects of DPF Cs-V-based non-noble metal catalysts and their coating forms on non-road diesel engine emission characteristics. *Environ. Sci. Pollut. Res.* **2023**, *30*, 9401–9415. [CrossRef] [PubMed]
36. Libby, W.F. Promising Catalyst for Auto Exhaust. *Science* **1971**, *171*, 499–500. [CrossRef] [PubMed]
37. Voorhoeve, R.J.H.; Remeika, J.P.; Freeland, P.E.; Matthias, B.T. Rare-Earth Oxides of Manganese and Cobalt Rival Platinum for the Treatment of Carbon Monoxide in Auto Exhaust. *Science* **1972**, *177*, 353–354. [CrossRef] [PubMed]
38. Legutko, P.; Stelmachowski, P.; Yu, X.; Zhao, Z.; Sojka, Z.; Kotarba, A. Catalytic Soot Combustion—General Concepts and Alkali Promotion. *ACS Catal.* **2023**, *13*, 3395–3418. [CrossRef]
39. Mei, X.; Xiong, J.; Wei, Y.; Zhang, Y.; Zhang, P.; Yu, Q.; Zhao, Z.; Liu, J. High-efficient non-noble metal catalysts of 3D ordered macroporous perovskite-type $La_2NiB'O_6$ for soot combustion: Insight into the synergistic effect of binary Ni and B′ sites. *Appl. Catal. B* **2020**, *275*, 119108. [CrossRef]
40. Xing, L.; Yang, Y.; Ren, W.; Zhao, D.; Tian, Y.; Ding, T.; Zhang, J.; Zheng, L.; Li, X. Highly efficient catalytic soot combustion performance of hierarchically meso-macroporous Co_3O_4/CeO_2 nanosheet monolithic catalysts. *Catal. Today* **2020**, *351*, 83–93. [CrossRef]
41. Stegmayer, M.Á.; Irusta, S.; Miró, E.E.; Milt, V.G. Electrospinning synthesis and characterization of nanofibers of Co, Ce and mixed Co-Ce oxides. Their application to oxidation reactions of diesel soot and CO. *Catal. Today* **2022**, *383*, 266–276. [CrossRef]
42. Xia, Y.; Wang, Z.; Feng, Y.; Xie, S.; Liu, Y.; Dai, H.; Deng, J. In situ molten salt derived iron oxide supported platinum catalyst with high catalytic performance for o-xylene elimination. *Catal. Today* **2020**, *351*, 30–36. [CrossRef]
43. Chi, H.; Zhang, P.; Xiong, J.; Wei, Y.; Li, Y.; Zhao, Z.; Liu, J.; Jiao, J. Single-crystalline α-MnO_2 catalysts with tailored exposed crystal facets for boosting catalytic soot oxidation: The crystal facet-dependent activity. *Appl. Surf. Sci.* **2023**, *608*, 155116. [CrossRef]
44. Zhai, G.; Wang, J.; Chen, Z.; Yang, S.; Men, Y. Highly enhanced soot oxidation activity over 3DOM Co_3O_4-CeO_2 catalysts by synergistic promoting effect. *J. Hazard. Mater.* **2019**, *363*, 214–226. [CrossRef] [PubMed]
45. Horyń, R.; Bukowska, E.; Sikora, A. Nature of structure defects in rhombohedral series of $La_{1-x}A_xMnO_{3+\delta}$ (A = Na, K). *J. Alloys Compd.* **2002**, *346*, 107–115. [CrossRef]
46. Liu, S.; Liu, Y.; Tang, D.; Miao, Y.; Cao, Z.; Zhao, Z. Synergy of NTP-$La_{1-x}Ag_xMn_{1-y}Co_yO_{3-\delta}$ Hybrid for Soot Catalytic Combustion at Low Temperature. *Plasma Chem. Plasma Process.* **2021**, *41*, 1009–1019. [CrossRef]
47. Uppara, H.P.; Singh, S.K.; Labhsetwar, N.K.; Murari, M.S.; Dasari, H. The decisive factor of hollow spherical network morphology of $Nd_{1-x}Ce_xCo_{1-y}Cu_yO_{3\pm\delta}$ perovskites towards soot oxidation. *Chem. Pap.* **2022**, *76*, 3771–3787. [CrossRef]
48. Cao, C.; Xing, L.; Yang, Y.; Tian, Y.; Ding, T.; Zhang, J.; Hu, T.; Zheng, L.; Li, X. The monolithic transition metal oxide crossed nanosheets used for diesel soot combustion under gravitational contact mode. *Appl. Surf. Sci.* **2017**, *406*, 245–253. [CrossRef]

49. Liu, Y.; Dai, H.; Du, Y.; Deng, J.; Zhang, L.; Zhao, Z.; Au, C.T. Controlled preparation and high catalytic performance of three-dimensionally ordered macroporous $LaMnO_3$ with nanovoid skeletons for the combustion of toluene. *J. Catal.* **2012**, *287*, 149–160. [CrossRef]
50. Xie, S.; Deng, J.; Zang, S.; Yang, H.; Guo, G.; Arandiyan, H.; Dai, H. Au–Pd/3DOM Co_3O_4: Highly active and stable nanocatalysts for toluene oxidation. *J. Catal.* **2015**, *322*, 38–48. [CrossRef]
51. Jin, B.; Wu, X.; Weng, D.; Liu, S.; Yu, T.; Zhao, Z.; Wei, Y. Roles of cobalt and cerium species in three-dimensionally ordered macroporous $Co_xCe_{1-x}O_\delta$ catalysts for the catalytic oxidation of diesel soot. *J. Colloid Interface Sci.* **2018**, *532*, 579–587. [CrossRef] [PubMed]
52. Tang, W.; Weng, J.; Lu, X.; Wen, L.; Suburamanian, A.; Nam, C.-Y.; Gao, P.-X. Alkali-metal poisoning effect of total CO and propane oxidation over Co_3O_4 nanocatalysts. *Appl. Catal. B* **2019**, *256*, 117859. [CrossRef]
53. Kostin, G.; Borodin, A.; Emely'anov, V.; Naumov, D.; Virovets, A.; Rohmer, M.M.; Varnek, A. Synthesis and structure of heterometallic compounds of $[RuNO(NO_2)_4OH]^{2-}$ with triphenyl phosphine oxide complexes of Co(II), Ni (II), and Zn(II). *J. Mol. Struct.* **2007**, *837*, 63–71. [CrossRef]
54. Chaisriratanakul, W.; Bunjongpru, W.; Pankiew, A.; Srisuwan, A.; Jeamsaksiri, W.; Chaowicharat, E.; Thornyanadacha, N.; Pengpad, P.; Horprathum, M.; Phromyothin, D. Modification of polyvinyl chloride ion-selective membrane for nitrate ISFET sensors. *Appl. Surf. Sci.* **2020**, *512*, 145664. [CrossRef]
55. Mihaylov, M.Y.; Ivanova, E.Z.; Aleksandrov, H.A.; Petkov, P.S.; Vayssilov, G.N.; Hadjiivanov, K.I. Species formed during NO adsorption and NO + O_2 co-adsorption on ceria: A combined DRIFTS and DFT study. *Mol. Catal.* **2018**, *451*, 114–124. [CrossRef]
56. Huang, H.Y.; Yang, R.T. Removal of NO by Reversible Adsorption on Fe−Mn Based Transition Metal Oxides. *Langmuir* **2001**, *17*, 4997–5003. [CrossRef]
57. Dai, X.; Jiang, W.; Wang, W.; Weng, X.; Shang, Y.; Xue, Y.; Wu, Z. Supercritical water syntheses of transition metal-doped CeO_2 nano-catalysts for selective catalytic reduction of NO by CO: An in situ diffuse reflectance Fourier transform infrared spectroscopy study. *Chin. J. Catal.* **2018**, *39*, 728–735. [CrossRef]
58. Mihaylov, M.; Hadjiivanov, K.; Panayotov, D. DRIFTS mechanistic studies on the selective catalytic reduction of NO_x with methane over Ni-containing zeolites: Comparison between NiY and Ni-ZSM-5. *Appl. Catal. B* **2004**, *51*, 33–42. [CrossRef]
59. Penkova, A.; Hadjiivanov, K.; Mihaylov, M.; Daturi, M.; Saussey, J.; Lavalley, J.C. DRIFTS Spectroscopic Study of Low Temperature NO Adsorption and NO + O_2 Coadsorption on H−ZSM-5. *Langmuir* **2004**, *20*, 5425–5431. [CrossRef]
60. Xue, H.; Guo, X.; Meng, T.; Mao, D.; Ma, Z. NH_3-SCR of NO over M/ZSM-5 (M = Mn, Co, Cu) catalysts: An in-situ DRIFTS study. *Surf. Interfaces* **2022**, *29*, 101722. [CrossRef]
61. Mihaylov, M.Y.; Zdravkova, V.R.; Ivanova, E.Z.; Aleksandrov, H.A.; Petkov, P.S.; Vayssilov, G.N.; Hadjiivanov, K.I. Infrared spectra of surface nitrates: Revision of the current opinions based on the case study of ceria. *J. Catal.* **2021**, *394*, 245–258. [CrossRef]
62. Mihaylov, M.Y.; Ivanova, E.Z.; Vayssilov, G.N.; Hadjiivanov, K.I. Revisiting ceria-NO_x interaction: DRIFTS studies. *Catal. Today* **2020**, *357*, 613–620. [CrossRef]